Supporting Information for:

Tuning Proton Kinetics in $BaCo_{0.4}Fe_{0.4}Zr_{0.2-X}Y_XO_{3-\delta}$ Triple Ionic-Electronic Conductors via Aliovalent Substitution

Jack H. Duffy, [a,b] Harry W. Abernathy, [b] Kyle S. Brinkman [a,b]

a. Department of Materials Science and Engineering, Clemson University, 515 Calhoun Drive, Clemson, SC 29634, USA. Email: jhduffy@clemson.edu

b. National Energy Technology Laboratory, United States Department of Energy, 3610 Collins Ferry Road, Morgantown, WV 26507, USA.

Pristine BCFZY$_X$ XRD:

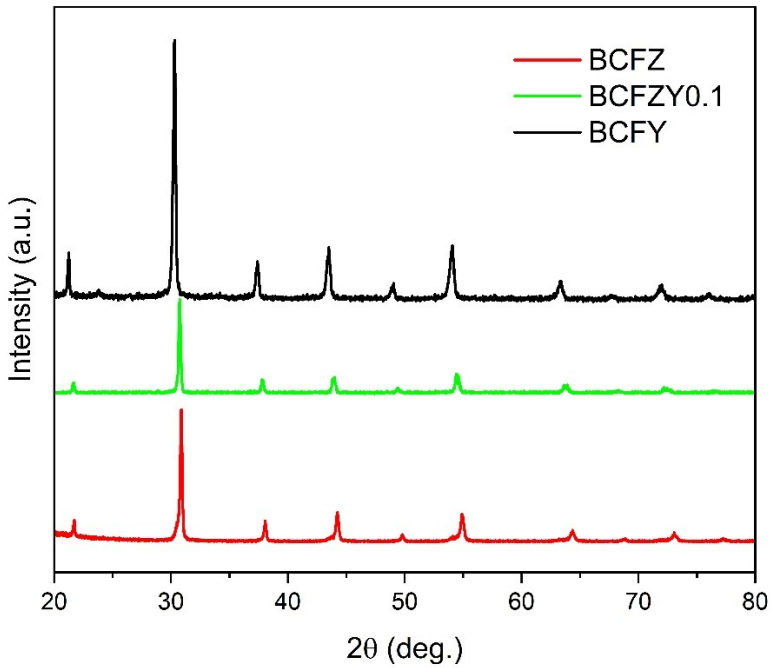

Figure S1: Comparison of XRD for pristine BCFZ, BCFZY0.1, and BCFY compositions, showing a general lattice parameter increase with increasing Y concentration.

Hydrogen permeation on bare membranes:

Based on the total conductivity measurements in the same atmosphere as the permeation measurements, a hysteresis occurs in the stabilization of conductivity after switching temperatures in 50°C increments, as shown in Figure S2. At lower temperatures, this hysteresis can take up to three hours, signifying the need for a period of stabilization for the hydrogen permeation membranes before sample measurements are taken. Initial measurements are therefore taken after this three-hour wait at each temperature. Over three different sampling periods at 600°C, the flux remains stable despite switching temperatures over a 50h permeation measurement as shown in Figure S3.

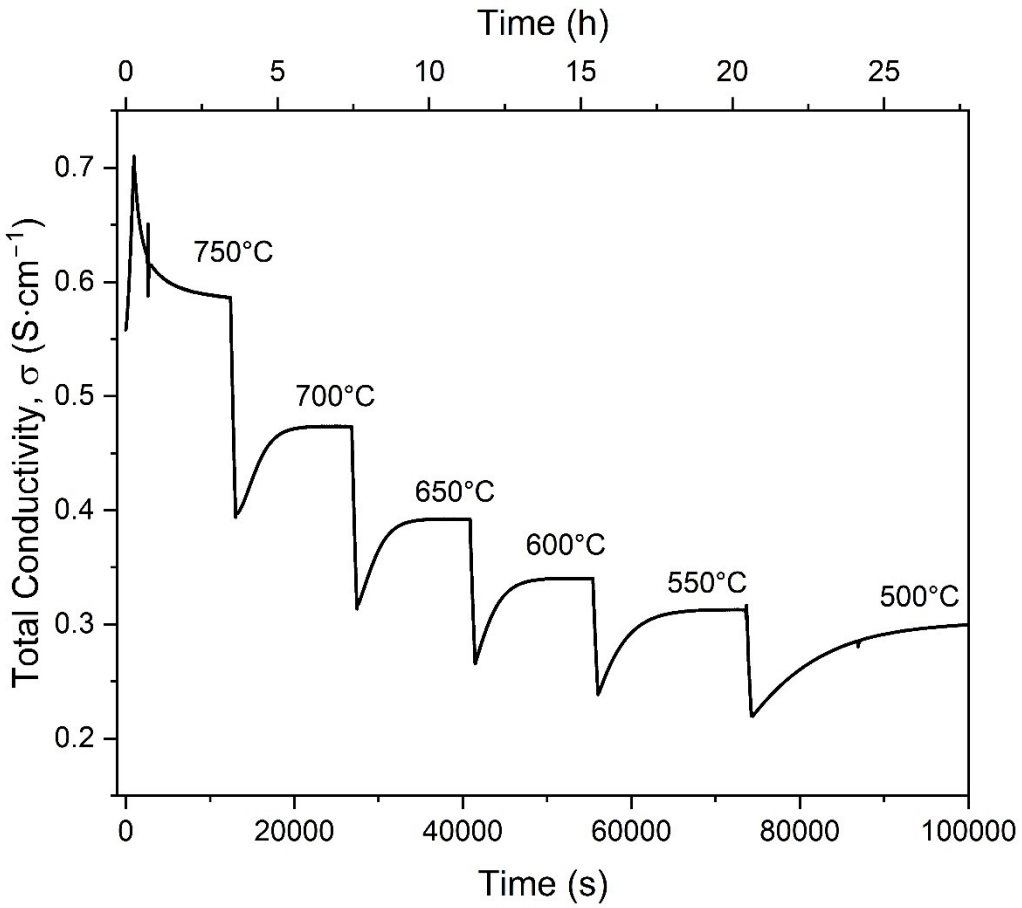

Figure S2: Total conductivity of BCFZY0.1 vs Time in reducing atmosphere, showing hysteresis when switching temperatures.

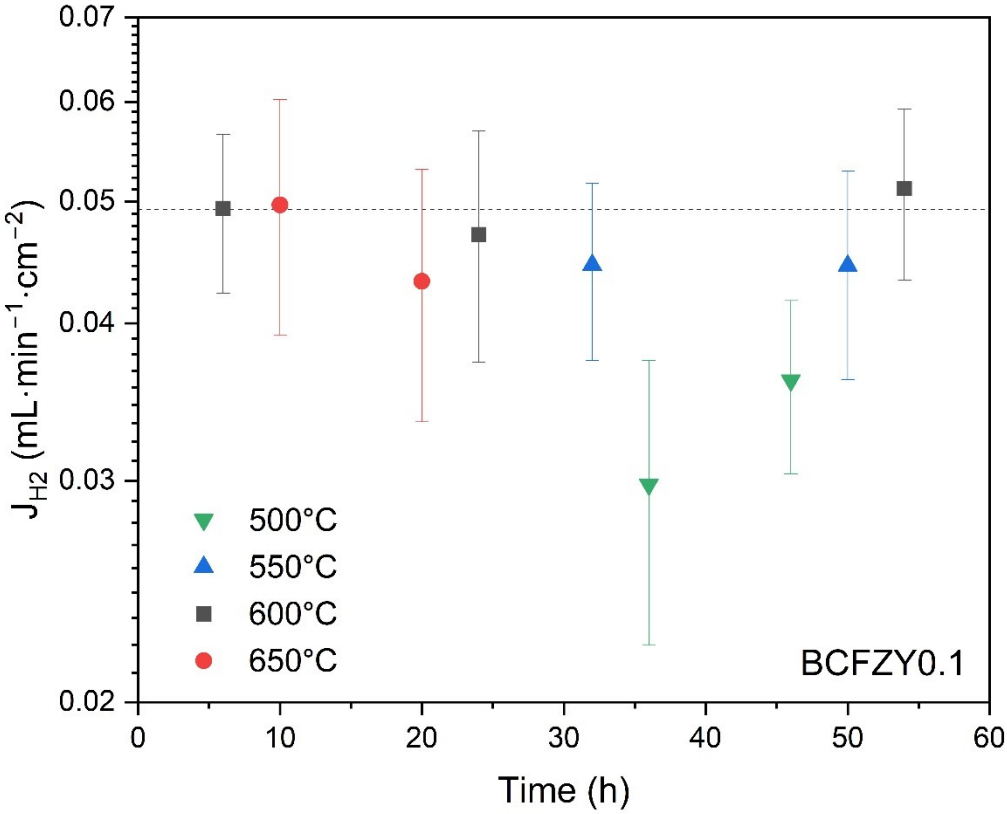

Figure S3: Hydrogen flux vs Time for BCFZY0.1, showing stable flux within the range of error at 600°C over 50h. Data points are taken from a one-hour sampling period from which the final five sampling points are averaged, with error bars taken from the propagation error of the measurement. Black dotted line serves as a guide to the eyes for the approximate flux at 600°C.

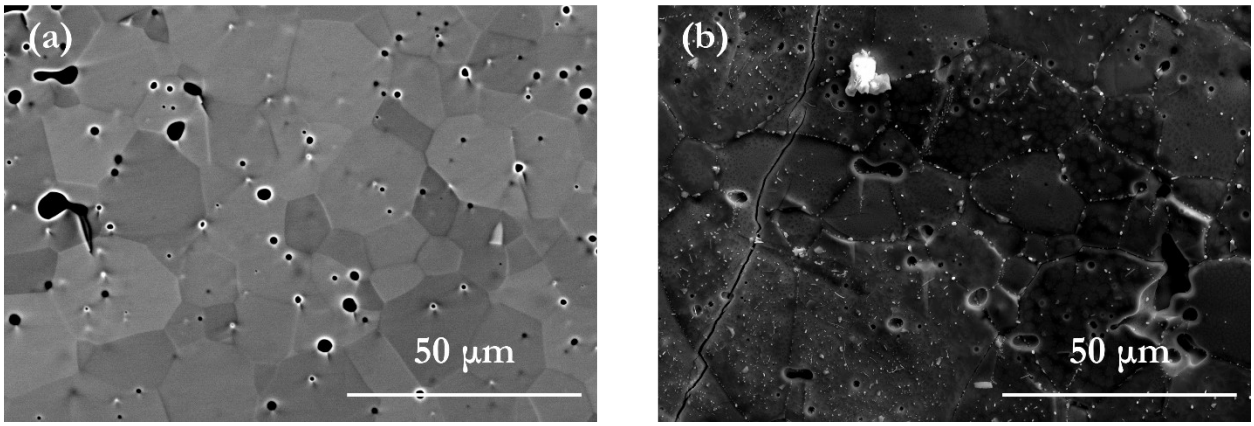

Figure S4: Cross-section SEM images of BCFZY0.1 showing (a) 5h and (b) 24h exposure times in 5% H_2 atmosphere. Small, bright dots indicating Co-rich phase appear after 24h exposure.

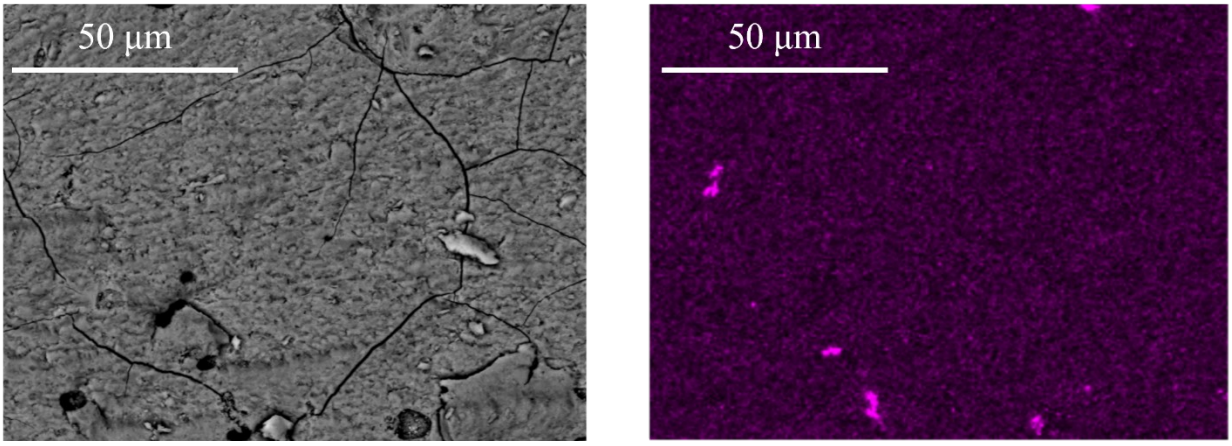

Figure S5: Cross-section SEM image of BCFZ with EDX of Cobalt, showing Co-rich phase appear after 50h exposure.

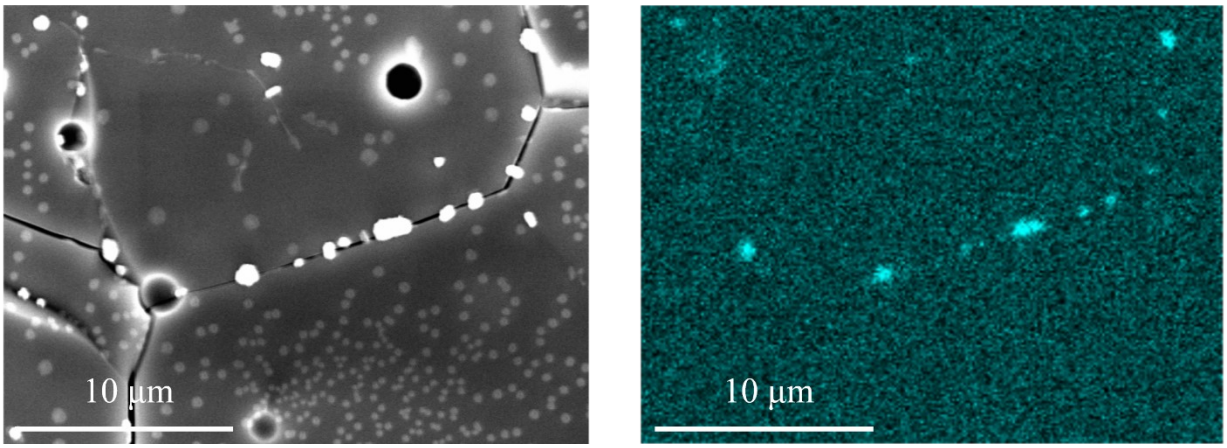

Figure S6: Cross-section SEM image of BCFZY0.1 with EDX of Cobalt, showing Co-rich phase appear after 50h exposure.

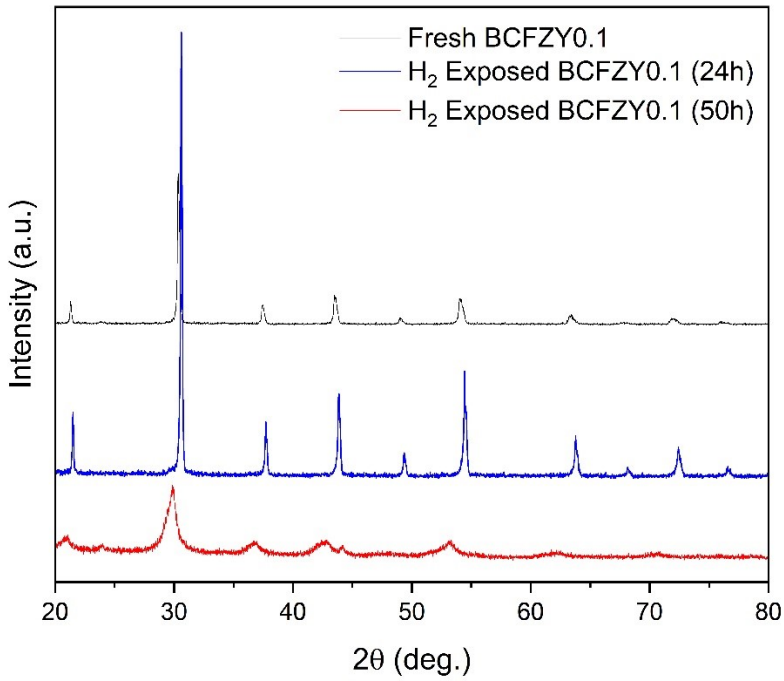

Figure S7: XRD for BCFZY0.1 for pristine, 24h-exposed, and 50h-exposed BCFZY0.1. Despite peak-broadening, the perovskite structure remains intact, and no significant change in permeation flux is observed.

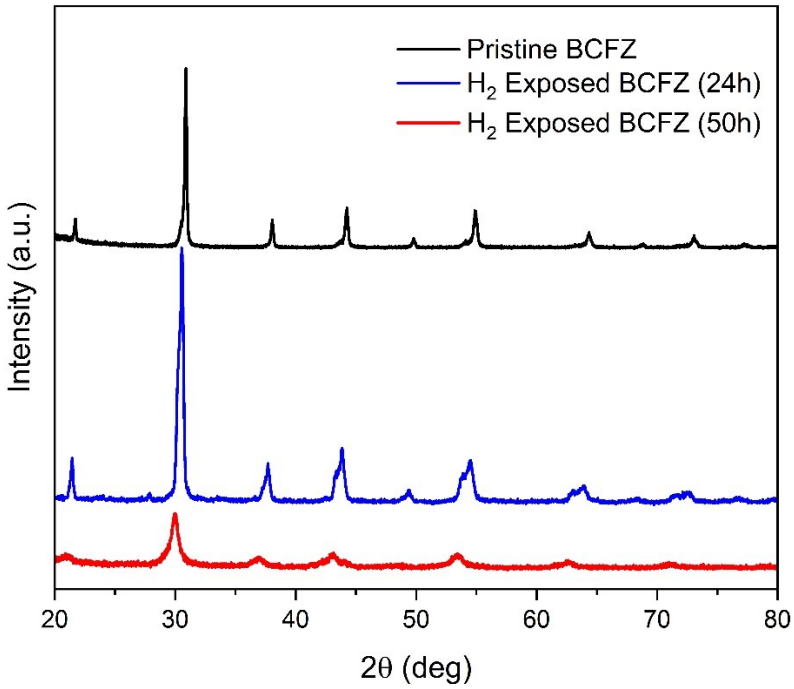

Figure S8: XRD for BCFZ for pristine, 24h-exposed, and 50h-exposed BCFZ. Peak splitting begins to show after 24h exposure, followed by peak-broadening at 50h exposure.

Palladium-Coated Membranes:

Deposition Procedure:

Pd was sputtered on each side of the $BCFZY_X$ membranes to achieve an approximately 500nm thickness. The deposition was performed at a target power of 67W from a 2" diameter target in a background pressure of 5 mTorr of Ar, flowing at 20 sccm, lasting about 20 minutes for each side. All samples were placed on a rotating plate during deposition. Following the deposition, the samples were annealed at 800°C for 3h in Ar atmosphere, with a heating rate of 5°C/min and a cooling rate of 2°C/min. Following the anneal, the sidewalls of each $BCFZY_X$ membrane were polished to remove excess palladium which could cause a short and allow protons only to transport through the palladium. This step was taken to ensure that $BCFZY_X$ was the limiting factor to proton transport.

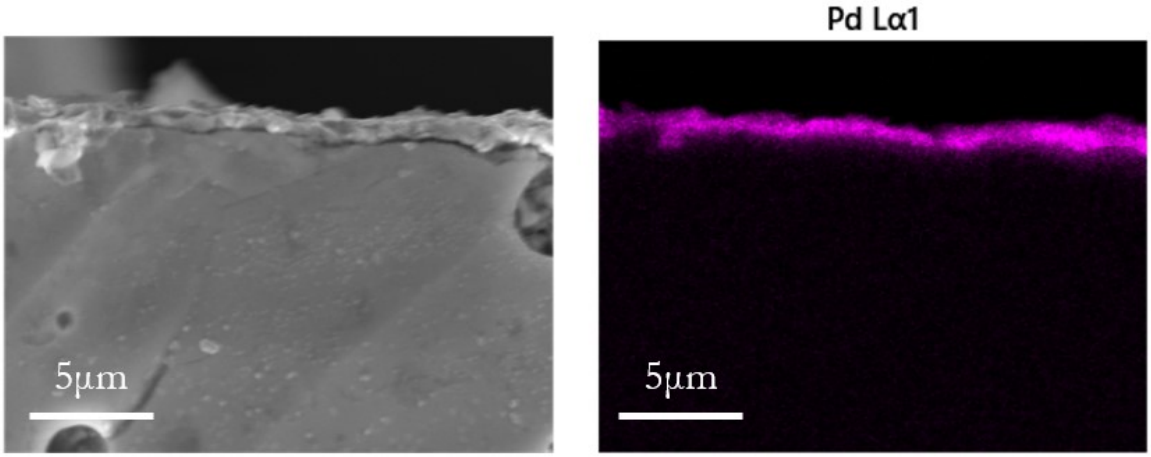

Figure S9: Cross-sectional SEM image of BCFZY0.1 membrane coated with a dense layer of palladium (approximately 500nm thickness), with EDX image confirming the composition of the dense layer.

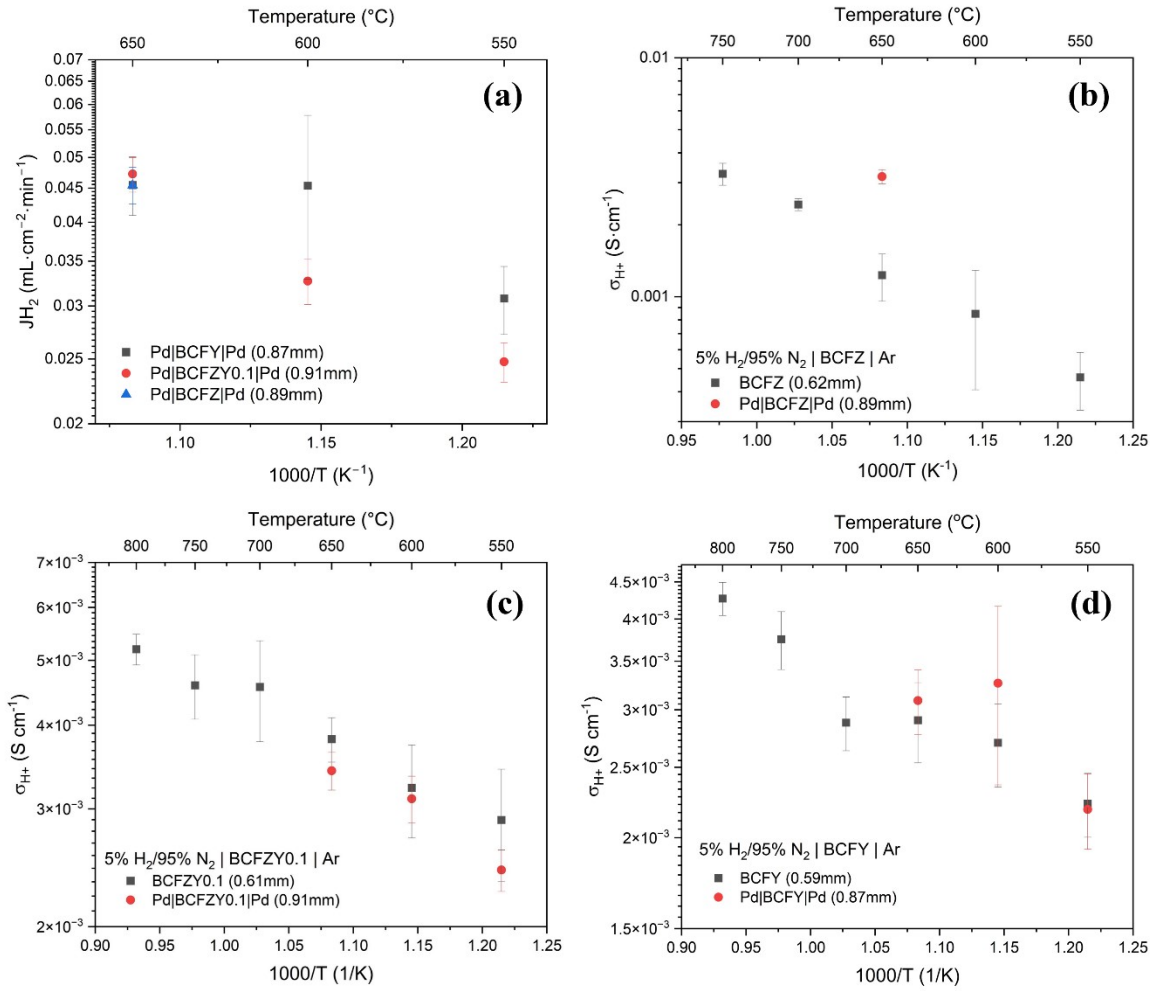

Figure S10: (a) Comparison of hydrogen flux for Pd-coated membranes. Comparison of estimated proton conductivity comparing bare and Pd-coated membranes for (b) BCFZ, (c) BCFZY0.1, and (d) BCFY.

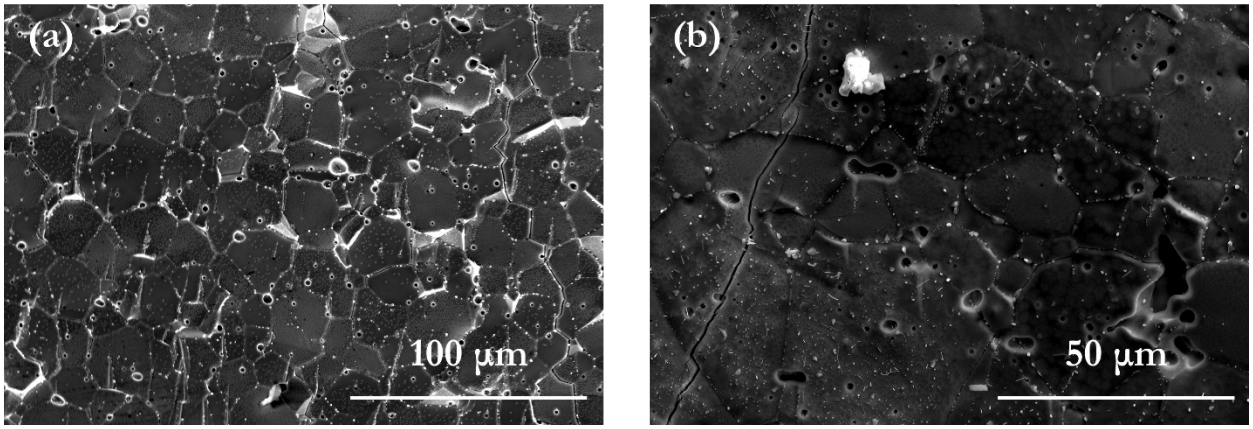

Figure S11: Cross-section SEM images after 5% H_2 exposure for (a) Pd-coated and (b) bare BCFZY0.1 membranes, both showing Co-rich nanoparticle segregation at grain boundaries.

Oxidation ECR fitting of $BCFZY_X$ compositions:

At high temperatures, BCFZ exhibits the best bulk-level oxygen reduction reaction in purely oxidative environments, which is attributed to the superior diffusivity of BCFZ coupled with a relatively small decrease in surface exchange coefficient; this results in the fastest relaxation. However, the advantage in diffusivity for BCFZ is quickly erased by the poor surface exchange coefficient at lower temperatures, and at 500°C, the relaxation time is more than double that of BCFZY0.1 and BCFY, greatly attributed to its poor k_{chem}. Meanwhile, despite its superior surface exchange coefficient, BCFY is always hindered compared to BCFZY0.1 because of its lower diffusivity, which is always lower by about a factor of two. This results in relaxation times which are about 40% longer at all temperatures. The ECR results suggest that BCFZY0.1 may exhibit the best properties as a cathode material for electrochemical devices in the low-to-intermediate-temperature range, while BCFZ may perform effectively in high-temperature devices. These results are shown in Figures S12 and S13 below:

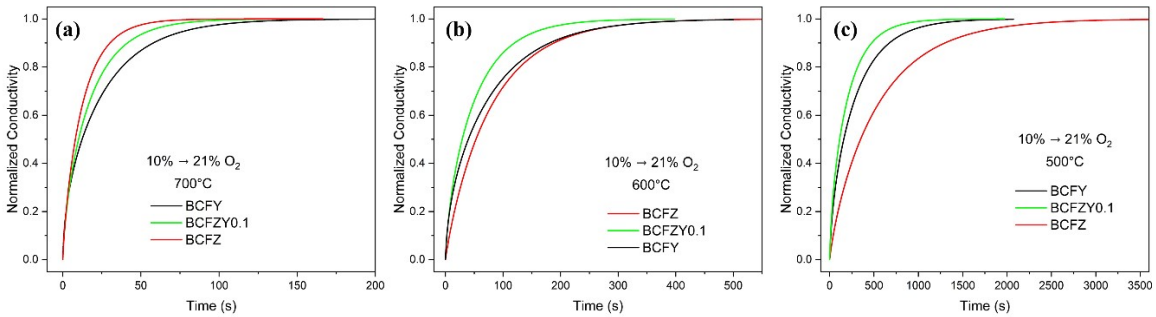

Figure S12: Fitted relaxation curves for $BCFZY_X$ materials at (a) 700°C, (b) 600°C, and (c) 500°C.

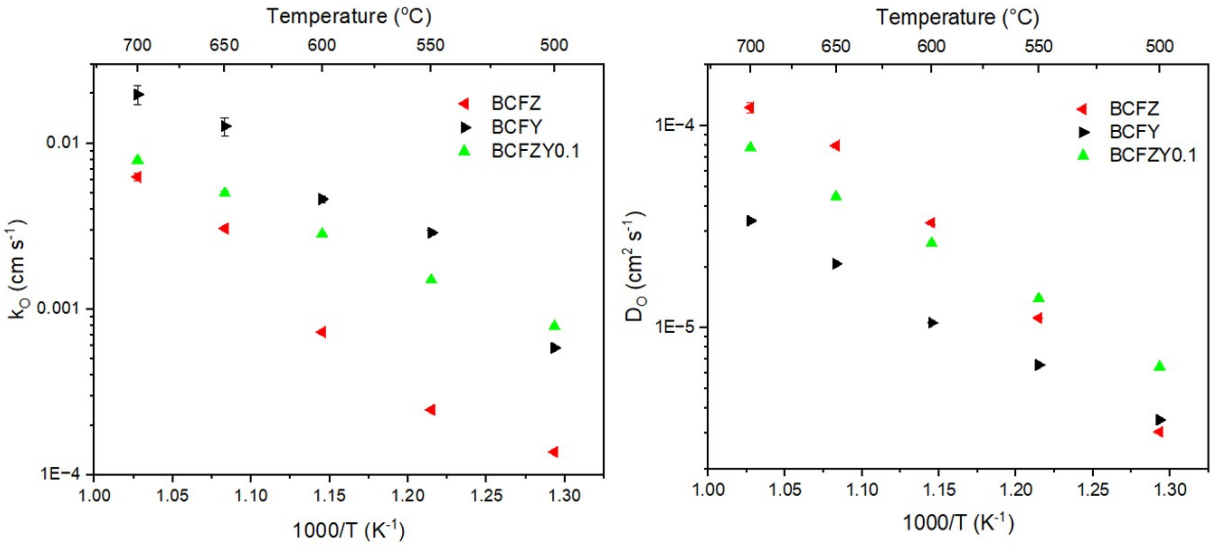

Figure S13: Fitting of (a) $k_{O,chem}$ and (b) $D_{O,chem}$ from ECR measurements for $BCFZY_X$ materials from 500-700°C in dry, oxidizing conditions, switching from 10% to 21% O_2 atmosphere.

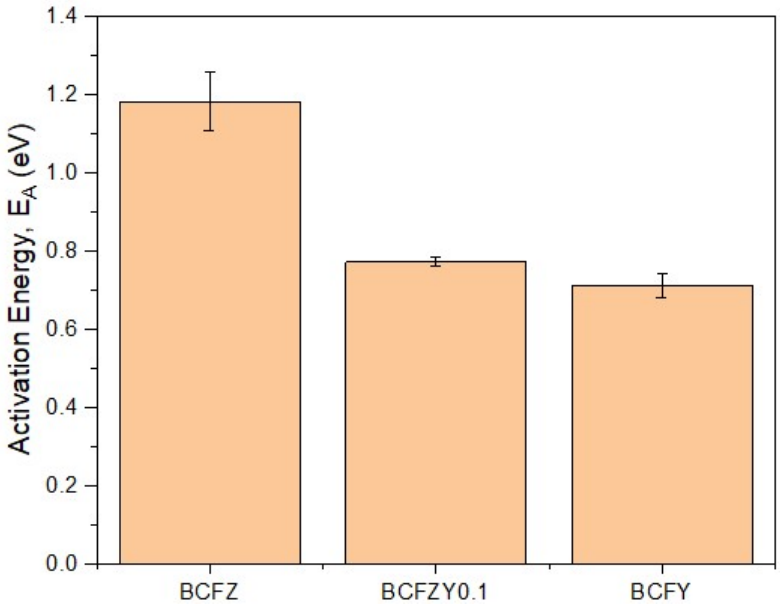

Figure S14: Comparison of the activation energy of $D_{O,\,chem}$ across the $BCFZY_X$ compositions.

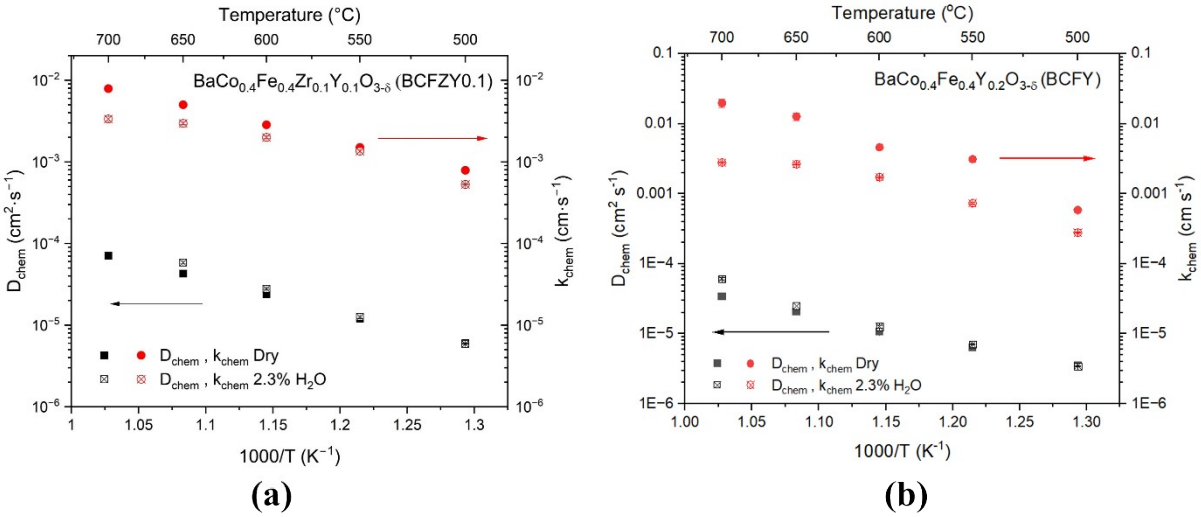

Figure S15: Fitting of $k_{O,chem}$ and $D_{O,chem}$ for dry and wet conditions for (a) BCFZY0.1, and (b) BCFY.